

Parameter dependence of two-fluid and finite Larmor radius effects on the Rayleigh-Taylor instability in finite beta plasmas

Cite as: Phys. Plasmas **23**, 122123 (2016); <https://doi.org/10.1063/1.4972819>

Submitted: 26 September 2016 • Accepted: 08 December 2016 • Published Online: 27 December 2016

 Atsushi Ito and Hideaki Miura



View Online



Export Citation



CrossMark

ARTICLES YOU MAY BE INTERESTED IN

[Two-fluid tearing mode instability in cylindrical geometry](#)

Phys. Plasmas **24**, 072102 (2017); <https://doi.org/10.1063/1.4986116>

[Numerical analysis of two-fluid tearing mode instability in a finite aspect ratio cylinder](#)

Phys. Plasmas **25**, 012117 (2018); <https://doi.org/10.1063/1.5009389>

[Amplitude and size scaling for interchange motions of plasma filaments](#)

Phys. Plasmas **23**, 122302 (2016); <https://doi.org/10.1063/1.4971220>

Physics of Plasmas

Papers from 62nd Annual Meeting of the
APS Division of Plasma Physics

Read now!



Parameter dependence of two-fluid and finite Larmor radius effects on the Rayleigh-Taylor instability in finite beta plasmas

Atsushi Ito and Hideaki Miura

National Institute for Fusion Science, National Institutes of Natural Sciences, 322-6 Oroshi-cho, Toki 509-5292, Japan

(Received 26 September 2016; accepted 8 December 2016; published online 27 December 2016)

The parameter dependence of two-fluid and finite Larmor radius (FLR) effects on the Rayleigh-Taylor (RT) instability in finite beta plasmas is examined based on extended magnetohydrodynamic (MHD) models. Four MHD models, the MHD model, two-fluid MHD model, MHD model with FLR effects, and two-fluid MHD model with FLR effects, are compared with each other with local and eigenmode analyses. For equilibria with nonuniform magnetic fields, the absence of complete stabilization of large wavenumber modes due to the FLR effect [Zhu *et al.*, Phys. Rev. Lett. **101**, 085005 (2008)] occurs for beta lower than the critical value for a small pressure gradient. For the two-fluid MHD model with the FLR term, it is shown that the absence of complete stabilization occurs for the beta different from that for the MHD model with the FLR term, the mode is not always most stable among those for the other models, depending on beta, and the coupling between RT mode and electron drift wave appears. The spatial dependence of the local analysis is examined in comparison with that of eigenfunctions. For the case of MHD with the FLR term, for large wavenumber modes, the growth rate of the eigenmode is larger than that of the local analysis at the center. In that case, the eigenfunction has two humps in the regions that are still unstable while the RT mode is completely stabilized at the center in the local analysis. *Published by AIP Publishing.* [<http://dx.doi.org/10.1063/1.4972819>]

I. INTRODUCTION

Small scale effects such as two-fluid and ion finite Larmor radius (FLR) effects are important for large wavenumber modes of magnetohydrodynamic (MHD) instabilities. It is known that large wavenumber modes of the Rayleigh-Taylor (RT) instability, or the interchange g-mode, are completely stabilized due to these small scale effects.¹ The fluid description that these small scale effects are added to MHD is called extended MHD. The two-fluid effect appears as the Hall current and the electron pressure gradient, and the FLR effect appears as the gyroviscosity in the extended MHD equations.¹⁻³ Simulation studies were also carried out⁴⁻⁶ based on extended MHD. A recent theory⁷ that extended the theory in Ref. 1 to finite beta and nonisothermal equilibrium showed that the complete stabilization is absent if the beta value exceeds a critical value. In the equilibrium used in Ref. 7 where a uniform magnetic field is assumed, the pressure gradient is fixed in order to balance with the gravitational force. The diamagnetic effects due to the two-fluid and FLR effects depend on the pressure gradient. Another aspect is the combination of the two-fluid and FLR effects on instability.⁸⁻¹² In Ref. 8, it is shown that the instability due to the two-fluid effect called the ion density gradient mode is stabilized by adding the FLR effect. Recent studies based on extended MHD equations for finite beta show that the growth rates of the RT mode are strongly reduced when both two-fluid and FLR effects are included^{9,10} and the effect is stronger for higher beta.¹⁰

In this study, we examine, by linear stability analysis, the effects of two-fluid and FLR on the RT instability in a wide range of parameters, such as the pressure and density

gradients, beta value, wavenumber, and space, to clarify the complicated behavior of the stability and diamagnetic effects due to two-fluid and FLR effects. We consider a nonuniform magnetic field to determine the pressure profile independent of the density profile. The linear eigenmode equations are derived and the local dispersion relation is obtained from them for the limit of the large wavenumber. The real frequencies of the RT instability due to diamagnetic effects vary depending on the pressure gradient. The absence of complete stabilization of large wavenumber modes due to the FLR effect occurs for beta values lower than the critical value when the pressure gradient is small. The value of the pressure gradient where the critical beta value coincides with the equilibrium beta limit is found. The combination of two-fluid and FLR effects can also cause the absence of complete stabilization and is not always most stable among the four models, MHD, two-fluid MHD, MHD with the FLR effect, and two-fluid MHD with the FLR effect, depending on beta. The two-fluid MHD with the FLR effect also shows coupling between the RT mode and the electron drift wave. The relation to the theory in Ref. 7 is also discussed. The spatial dependence of the local analysis is examined in comparison with that of eigenfunctions. For the case of MHD with the FLR effect, for large wavenumber modes, the growth rate of the eigenmode is larger than that of the local analysis at the center. In that case, the eigenfunction has two humps in the regions that are still unstable while the RT mode is completely stabilized at the center in the local analysis.

This paper is organized as follows. In Sec. II, we introduce eigenmode equations for RT instability based on extended MHD. In Sec. III, we present dependence of the RT instability

on parameters based on local analysis. In Sec. IV, we present eigenmode analysis and compare it with local analysis. The summary is given in Sec. V.

II. EIGENMODE EQUATIONS BASED ON EXTENDED MHD

We derive linear eigenmode equations for RT instability based on extended MHD. The extended MHD equations are

$$\frac{\partial n}{\partial t} + \nabla \cdot (n\mathbf{v}) = 0, \quad (1)$$

$$m_i n \left(\frac{\partial \mathbf{v}}{\partial t} + \mathbf{v} \cdot \nabla \mathbf{v} \right) = \mathbf{j} \times \mathbf{B} - \nabla p + m_i n \mathbf{g} - \delta \nabla \cdot \Pi_i^{gv}, \quad (2)$$

$$\mathbf{E} + \mathbf{v} \times \mathbf{B} - \frac{\lambda}{ne} (\mathbf{j} \times \mathbf{B} - \nabla p_e) = 0, \quad (3)$$

$$\frac{\partial \mathbf{B}}{\partial t} + \nabla \times \mathbf{E} = 0, \quad (4)$$

$$\mu_0 \mathbf{j} = \nabla \times \mathbf{B}, \quad (5)$$

where n is the density for ions and electrons with charge neutrality, \mathbf{v} is the ion flow velocity, m_i is the ion mass, e is the electric charge, \mathbf{j} is the current density, \mathbf{B} is the magnetic field, \mathbf{E} is the electric field, Π_i^{gv} is the ion gyroviscous tensor, and p_i and p_e are the ion and electron pressures. We consider two-fluid and ion FLR effects, while inertia and FLR effects of electrons are neglected since $m_i \gg m_e$, where m_e is the electron mass. The last term on the right-hand side (RHS) of the equation of motion (2) is the ion gyroviscous force that appears due to the FLR effect.² The last term on the left-hand side (LHS) of the generalized Ohm's law (3) includes the Hall current and electron pressure due to the two-fluid effect. We have introduced the artificial indices λ and δ that label the two-fluid, ion FLR terms, respectively: $(\lambda, \delta) = (0, 0)$ for the single-fluid (ideal) MHD (MHD model), $(0, 1)$ for the MHD with the FLR term (FLR model), $(1, 0)$ for the two-fluid MHD (TF model), and $(1, 1)$ for the two-fluid MHD with the FLR term (TF+FLR model). We use a simple model for pressure as in Ref. 7 that is the adiabatic equation for total pressure $p = p_i + p_e$

$$\frac{\partial p}{\partial t} + \mathbf{v} \cdot \nabla p + \gamma p \nabla \cdot \mathbf{v} = 0, \quad (6)$$

with

$$p_i/p = \tau, \quad \tau = \text{const.}, \quad (7)$$

where $\gamma = 5/3$ and pressure anisotropy and heat fluxes are neglected. The gyroviscous force in general magnetic configuration,¹³ neglecting pressure anisotropy and heat fluxes, is given by

$$\begin{aligned} \nabla \cdot \Pi_i^{gv} = & -m_i n \mathbf{v}_{*i} \cdot \nabla \mathbf{v} - \nabla \chi_v - \nabla \\ & \times \left\{ \frac{m_i p_i}{e B^2} \left\{ \mathbf{B} \cdot \nabla \mathbf{v} + \frac{1}{2} \left[\nabla \cdot \mathbf{v} - \frac{3}{B^2} \mathbf{B} \cdot (\mathbf{B} \cdot \nabla \mathbf{v}) \right] \mathbf{B} \right\} \right\} \\ & + \mathbf{B} \cdot \nabla \left\{ \frac{m_i p_i}{e B^4} \mathbf{B} \times [3 \mathbf{B} \cdot \nabla \mathbf{v} + \mathbf{B} \times (\nabla \times \mathbf{v})] + \frac{\chi_v}{B^2} \mathbf{B} \right\}, \end{aligned} \quad (8)$$

where $B = |\mathbf{B}|$

$$\mathbf{v}_{*i} = -\frac{1}{en} \nabla \times \left(\frac{p_i}{B^2} \mathbf{B} \right), \quad (9)$$

$$\chi_v = \frac{m_i p_i}{2e B^2} \mathbf{B} \cdot (\nabla \times \mathbf{v}). \quad (10)$$

Here, we linearize the above extended MHD equations. We consider static equilibrium in slab geometry (x, y, z) . The gravity and nonuniformity of equilibrium quantities are in the x -direction, and the equilibrium magnetic field is in z

$$\mathbf{g} = g \mathbf{e}_x, \quad g = \text{const.}, \quad (11)$$

$$n_0 = n_0(x), \quad (12)$$

$$p_0 = p_0(x), \quad (13)$$

$$\mathbf{B}_0 = B_0(x) \mathbf{e}_z, \quad (14)$$

$$\mathbf{v}_0 = 0, \quad (15)$$

$$p_{i0} = \tau p_0, \quad (16)$$

$$p_{e0} = (1 - \tau) p_0, \quad (17)$$

where 0 denotes equilibrium quantities. It is noted that equilibrium flow \mathbf{v}_0 is zero means that $E \times B$ and other drifts are cancelled. The equilibrium force balance is

$$\left(p_0 + \frac{B_0^2}{2\mu_0} \right)' = m_i n_0 g, \quad (18)$$

where the prime denotes d/dx . We linearize with the perturbations of the form

$$f_1 = f_1(x) \exp(iky - i\omega t). \quad (19)$$

We assume flute perturbation $\mathbf{v}_1 = (v_{1x}, v_{1y}, 0)$, while $\mathbf{B}_1 = (B_{1x}, B_{1y}, B_{1z})$. The linearized equations are

$$\begin{aligned} -im_i n_0 \left[\omega + \frac{\delta k}{2en_0} \left(\frac{p_{i0}}{B_0} \right)' \right] v_{1x} \\ = -p_1' - \mu_0^{-1} (B_0 B_{1z}' + B_0' B_{1z}) + m_i g n_1 \\ + \frac{\delta m_i}{2e} \left[\frac{p_{i0}}{B_0} (v_{1y}'' - k^2 v_{1y}) + \left(\frac{p_{i0}}{B_0} \right)' v_{1y}' \right], \end{aligned} \quad (20)$$

$$\begin{aligned} -im_i n_0 \left[\omega + \frac{\delta k}{2en_0} \left(\frac{p_{i0}}{B_0} \right)' \right] v_{1y} \\ = -ik p_1 - i\mu_0^{-1} k B_0 B_{1z} \\ - \frac{\delta m_i}{2e} \left[\frac{p_{i0}}{B_0} (v_{1x}'' - k^2 v_{1x}) + \left(\frac{p_{i0}}{B_0} \right)' v_{1x}' \right], \end{aligned} \quad (21)$$

$$-i\omega B_{1z} = ik E_{1x} - E_{1y}', \quad (22)$$

$$E_{1x} = -B_0 v_{1y}$$

$$+ \frac{\lambda}{n_0 e} \left[\left(\frac{B_0^2}{2\mu_0} + p_{e0} \right)' \frac{n_1}{n_0} - \frac{1}{\mu_0} (B_0 B_{1z})' - p_{e1}' \right], \quad (23)$$

$$E_{1y} = B_0 v_{1x} - \frac{i\lambda k}{n_0 e} \left(\frac{B_0}{\mu_0} B_{1z} + p_{e1} \right), \quad (24)$$

$$-i\omega p_1 + p'_0 v_{1x} = -\gamma p_0 (v'_{1x} + i k v_{1y}), \quad (25)$$

$$-i\omega n_1 + n'_0 v_{1x} = -n_0 (v'_{1x} + i k v_{1y}), \quad (26)$$

$$p_{e1} = (1 - \tau) p_1. \quad (27)$$

It is noted that, in this simple system, the expression of gyroviscosity (8) does not make a difference in linearized equations from those derived with the simple expression of gyroviscosity in Refs. 1 and 7. We normalize the quantities as $\mathbf{B} = B_* \bar{\mathbf{B}}$, $n = n_* \bar{n}$, $p = (B_*^2 / \mu_0) \bar{p}$, $\mathbf{v} = V_{Ac} \bar{\mathbf{v}}$, $x = L \bar{x}$, $\omega = (V_{Ac} / L) \bar{\omega}$, and $k = \bar{k} / L$ where B_* , n_* , and L are characteristic of the magnetic field, density, and length, respectively, and

$$V_{Ac} = \frac{B_*}{\sqrt{\mu_0 n_* m_i}} \quad (28)$$

is the Alfvén velocity. Eliminating variables without using any ordering, we obtain two coupled second-order ordinary differential equations (ODEs) for v_{x1} and v_{y1}

$$A_1(\bar{x}) \bar{v}''_{1x} + B_1(\bar{x}) \bar{v}'_{1x} + C_1(\bar{x}) \bar{v}_{1x} + D_1(\bar{x}) \bar{v}''_{1y} + E_1(\bar{x}) \bar{v}'_{1y} + F_1(\bar{x}) \bar{v}_{1y} = 0, \quad (29)$$

$$A_2(\bar{x}) \bar{v}''_{1x} + B_2(\bar{x}) \bar{v}'_{1x} + C_2(\bar{x}) \bar{v}_{1x} + F_2(\bar{x}) \bar{v}_{1y} = 0, \quad (30)$$

$$A_1(\bar{x}) = i \left\{ \gamma \bar{p}_0 + \bar{B}_0^2 + \lambda \bar{k} \frac{d_i \bar{B}_0}{L \bar{n}_0} \left(\bar{\omega} - \lambda \bar{k} \frac{d_i \bar{n}'_0}{L \bar{n}_0^2} \bar{B}_0 \right)^{-1} \times \left[\bar{B}_0^2 \left(\frac{\bar{n}'_0}{\bar{n}_0} - \frac{\bar{B}'_0}{\bar{B}_0} \right) + (1 - \tau) \left(\frac{\bar{n}'_0}{\bar{n}_0} \gamma \bar{p}_0 - \bar{p}'_0 \right) \right] \right\}, \quad (31)$$

$$B_1(\bar{x}) = i \left\{ \gamma \bar{p}'_0 + 2 \bar{B}_0 \bar{B}'_0 + \lambda \bar{k} \frac{d_i}{L \bar{n}_0 \bar{B}_0} \left(\bar{\omega} - \lambda \bar{k} \frac{d_i \bar{n}'_0}{L \bar{n}_0^2} \bar{B}_0 \right)^{-1} \times \left\{ \bar{B}_0^2 \left[(1 - \tau) \frac{\gamma}{\bar{n}_0} \left[\left(-\frac{2 \bar{n}'_0}{\bar{n}_0} - \frac{\bar{B}'_0}{\bar{B}_0} \right) \bar{n}'_0 \bar{p}_0 + \bar{n}''_0 \bar{p}_0 + \bar{n}'_0 \bar{p}'_0 \right] - \bar{B}_0 \bar{B}''_0 + (1 - \tau) \left[\left(\frac{\bar{n}'_0}{\bar{n}_0} + \frac{\bar{B}'_0}{\bar{B}_0} \right) \bar{p}'_0 - \bar{p}''_0 \right] + \frac{\bar{B}_0^2}{\bar{n}_0} \left[2 \bar{n}'_0 \left(-\frac{\bar{n}'_0}{\bar{n}_0} + \frac{\bar{B}'_0}{\bar{B}_0} \right) + \bar{n}''_0 \right] \right\} + \left\{ \frac{\bar{n}'_0}{\bar{n}_0} \left[\gamma (1 - \tau) \bar{p}_0 + \bar{B}_0^2 \right] - \bar{B}_0 \bar{B}'_0 - (1 - \tau) \bar{p}'_0 \right\} \times \left[2 \bar{B}_0 \bar{B}'_0 + \lambda \bar{k} \frac{d_i \bar{B}_0}{L \bar{n}_0^2} \left(\bar{\omega} - \lambda \bar{k} \frac{d_i \bar{n}'_0}{L \bar{n}_0^2} \bar{B}_0 \right)^{-1} \times \left(\bar{n}''_0 \bar{B}_0 + \bar{n}'_0 \bar{B}'_0 - \frac{2 \bar{n}'_0}{\bar{n}_0} \bar{B}_0 \right) \right] \right\}, \quad (32)$$

$$C_1(\bar{x}) = i \left[\bar{n}_0 \bar{\omega}^2 + \frac{\delta d_i}{2 L} \tau \frac{k \bar{\omega}}{\bar{B}_0} \left(\bar{p}'_0 - \frac{\bar{B}'_0}{\bar{B}_0} \bar{p}_0 \right) \right], \quad (33)$$

$$D_1(\bar{x}) = \frac{\delta}{2} \tau \frac{d_i \bar{p}_0}{L \bar{B}_0} \bar{\omega}, \quad (34)$$

$$E_1(\bar{x}) = -k \gamma \bar{p}_0 + \frac{\delta}{2} \tau \frac{d_i \bar{\omega}}{L \bar{B}_0} \left(\bar{p}'_0 - \frac{\bar{B}'_0}{\bar{B}_0} \bar{p}_0 \right) - k \bar{B}_0^2 - \lambda \bar{k}^2 \frac{d_i \bar{B}_0}{L \bar{n}_0} \left(\bar{\omega} - \lambda \bar{k} \frac{d_i \bar{n}'_0}{L \bar{n}_0^2} \bar{B}_0 \right)^{-1} \times \left[\bar{B}_0^2 \left(\frac{\bar{n}'_0}{\bar{n}_0} - \frac{\bar{B}'_0}{\bar{B}_0} \right) + (1 - \tau) \left(\frac{\bar{n}'_0}{\bar{n}_0} \gamma \bar{p}_0 - \bar{p}'_0 \right) \right], \quad (35)$$

$$F_1(\bar{x}) = k \left(-\gamma \bar{p}'_0 - \frac{\delta d_i}{2 L} \tau \frac{\bar{p}_0}{\bar{B}_0} k \bar{\omega} + \frac{L g}{V_{Ac}^2} \bar{n}_0 - 2 \bar{B}_0 \bar{B}'_0 \right) - \lambda \bar{k}^2 \frac{d_i \bar{B}_0}{L \bar{n}_0} \left(\bar{\omega} - \lambda \bar{k} \frac{d_i \bar{n}'_0}{L \bar{n}_0^2} \bar{B}_0 \right)^{-1} \left\{ \bar{B}_0^2 \left[\frac{\bar{B}'_0}{\bar{B}_0} - \frac{\bar{n}'_0}{\bar{n}_0} + \lambda \bar{k} \frac{d_i \bar{B}_0}{L \bar{n}_0^2} \left(\bar{\omega} - \lambda \bar{k} \frac{d_i \bar{n}'_0}{L \bar{n}_0^2} \bar{B}_0 \right)^{-1} \left(\bar{n}'_0 \frac{\bar{B}'_0}{\bar{B}_0} + \bar{n}''_0 - \frac{2 \bar{n}'_0}{\bar{n}_0} \right) \right] \times \left[\bar{B}_0^2 \left(\frac{\bar{n}'_0}{\bar{n}_0} - \frac{\bar{B}'_0}{\bar{B}_0} \right) + (1 - \tau) \left(\frac{\bar{n}'_0}{\bar{n}_0} \gamma \bar{p}_0 - \bar{p}'_0 \right) \right] + \bar{B}_0^2 \left\{ \bar{B}_0 \bar{B}'_0 \left(\frac{2 \bar{n}'_0}{\bar{n}_0} - \frac{\bar{B}'_0}{\bar{B}_0} \right) - \bar{B}_0 \bar{B}''_0 + \frac{\bar{B}_0^2}{\bar{n}_0} \left(\bar{n}''_0 - \frac{\bar{n}'_0}{\bar{n}_0} \right) + (1 - \tau) \left[\frac{\gamma \bar{p}_0}{\bar{n}_0} \left(\bar{n}'_0 - \frac{\bar{n}'_0}{\bar{n}_0} \right) + \frac{\bar{n}'_0}{\bar{n}_0} \gamma \bar{p}'_0 - \bar{p}''_0 \right] \right\} \right\}, \quad (36)$$

$$A_2(\bar{x}) = \frac{\delta}{2} \tau \frac{d_i \bar{p}_0}{L \bar{B}_0} \bar{\omega}, \quad (37)$$

$$B_2(\bar{x}) = \frac{\delta}{2} \tau \frac{d_i \bar{\omega}}{L \bar{B}_0} \left(\bar{p}'_0 - \frac{\bar{B}'_0}{\bar{B}_0} \bar{p}_0 \right) + k \gamma \bar{p}_0 + k \bar{B}_0^2 + \lambda \bar{k}^2 \frac{d_i \bar{B}_0}{L \bar{n}_0} \left(\bar{\omega} - \lambda \bar{k} \frac{d_i \bar{n}'_0}{L \bar{n}_0^2} \bar{B}_0 \right)^{-1} \times \left[\bar{B}_0^2 \left(\frac{\bar{n}'_0}{\bar{n}_0} - \frac{\bar{B}'_0}{\bar{B}_0} \right) + (1 - \tau) \left(\frac{\bar{n}'_0}{\bar{n}_0} \gamma \bar{p}_0 - \bar{p}'_0 \right) \right], \quad (38)$$

$$C_2(\bar{x}) = -\frac{\delta}{2} \tau \frac{d_i \bar{p}_0}{L \bar{B}_0} \bar{k}^2 \bar{\omega} + \bar{k} \bar{p}'_0 + \bar{k} \bar{B}_0 \bar{B}'_0, \quad (39)$$

$$F_2(\bar{x}) = -i \left\{ \bar{n}_0 \bar{\omega}^2 + \frac{\delta}{2} \tau \frac{d_i \bar{\omega}}{L \bar{B}_0} \left(\bar{p}'_0 - \frac{\bar{B}'_0}{\bar{B}_0} \bar{p}_0 \right) - \bar{k}^2 \left(\gamma \bar{p}_0 + \bar{B}_0^2 \right) - \lambda \bar{k}^3 \frac{d_i \bar{B}_0}{L \bar{n}_0} \left(\bar{\omega} - \lambda \bar{k} \frac{d_i \bar{n}'_0}{L \bar{n}_0^2} \bar{B}_0 \right)^{-1} \times \left[\bar{B}_0^2 \left(\frac{\bar{n}'_0}{\bar{n}_0} - \frac{\bar{B}'_0}{\bar{B}_0} \right) + (1 - \tau) \left(\frac{\bar{n}'_0}{\bar{n}_0} \gamma \bar{p}_0 - \bar{p}'_0 \right) \right] \right\}, \quad (40)$$

where

$$d_i = \sqrt{\frac{m_i}{\mu_0 n_* e^2}} \quad (41)$$

is the ion skin depth. In the following, overbars are omitted. We consider the following equilibrium profiles

$$P'_0 = \frac{Lg}{V_{Ac}^2} n_0, \quad (42)$$

$$p_0 + \frac{B_0^2}{2} = P_0, \quad (43)$$

$$n_0 = \frac{n_1 + n_2}{2} + \frac{n_2 - n_1}{2} \tanh\left(\frac{2x}{x_2 - x_1}\right), \quad (44)$$

$$P_0 = \frac{B_Z^2}{2} + \frac{Lg}{V_{Ac}^2} \left[\frac{n_1 + n_2}{2} x + \frac{1}{4} (n_2 - n_1) (x_2 - x_1) \times \log \cosh\left(\frac{2x}{x_2 - x_1}\right) \right], \quad (45)$$

$$p_0 = \beta \left[\frac{p_1 + p_2}{2} + \frac{p_2 - p_1}{2} \tanh\left(\frac{2x}{x_2 - x_1}\right) \right], \quad (46)$$

$$B_0 = \sqrt{2(P_0 - p_0)}. \quad (47)$$

These are the same as those used in Ref. 10. The equilibrium temperature and magnetic field B_0 can be nonuniform. The RT instability occurs when

$$\frac{Lg}{V_{Ac}^2} \frac{n'_0}{n_0} < 0. \quad (48)$$

Figure 1 shows an example of equilibrium profiles of n_0 , p_0 , and B_0 . In the following analysis we fix $x_1 = -0.5$, $x_2 = 0.5$, $n_1 = 1.0$, $p_1 = 1.0$, $\tau = 0.5$, $B_Z = 1.0$, $Lg/V_{Ac}^2 = -0.01$, and $d_i/L = 0.2$, and examine dependence of RT mode in each model on the density and pressure gradients and the beta value by changing n_2 , p_2 , and β .

The two-fluid and FLR effects have the scale lengths of the ion skin depth d_i and the Larmor radius of ions

$$\rho_i = \frac{m_i v_{ii}}{eB} = \frac{1}{eB} \sqrt{\frac{m_i p_i}{n}} \sim d_i \sqrt{\tau \beta}, \quad (49)$$

respectively, and cannot be neglected for large wavenumber modes where $k(d_i/L)$ and $k(\rho_i/L)$, respectively, become finite. Since Eq. (49) shows that the ion Larmor radius ρ_i is proportional to the ion skin depth d_i , MHD with FLR cannot be produced with $d_i/L = 0$ but with $d_i/L \neq 0$ and $(\lambda, \delta) = (0, 1)$. The fluid description with the gyroviscosity requires small $k(\rho_i/L)$. However, since nonlinear extended MHD simulations include large wavenumber modes, the understanding of those modes is needed.

III. LOCAL ANALYSIS

From Equations (29) and (30), eliminating v_{y1} , we obtain the following fourth order ODE for v_{1x} ,

$$\begin{aligned} & -A_2 D_1 v_{1x}'''' + \left[D_1 \left(\frac{2F'_2 A_2}{F_2} - 2A'_2 - B_2 \right) - A_2 E_1 \right] v_{1x}'''' \\ & + \left\{ A_1 F_2 + D_1 \left[-\frac{F'_2}{F_2} \left(\frac{F'_2 A_2}{F_2} - A'_2 - B_2 \right) \right. \right. \\ & + \left. \left. \left(\frac{F'_2 A_2}{F_2} - A'_2 - B_2 \right)' + \frac{F'_2 B_2}{F_2} - B'_2 - C_2 \right] \right. \\ & + E_1 \left(\frac{F'_2 A_2}{F_2} - A'_2 - B_2 \right) - F_1 A_2 \} v_{1x}'' + \left\{ B_1 F_2 + D_1 \right. \\ & \times \left[-\frac{F'_2}{F_2} \left(\frac{F'_2 B_2}{F_2} - B'_2 - C_2 \right) + \left(\frac{F'_2 B_2}{F_2} - B'_2 - C_2 \right)' \right. \\ & + \left. \left. \frac{F'_2 C_2}{F_2} - C'_2 \right] + E_1 \left(\frac{F'_2 B_2}{F_2} - B'_2 - C_2 \right) - F_1 B_2 \} v_{1x}' \right. \\ & + \left. \left\{ C_1 F_2 + D_1 \left[-\frac{F'_2}{F_2} \left(\frac{F'_2 C_2}{F_2} - C'_2 \right) + \left(\frac{F'_2 C_2}{F_2} - C'_2 \right)' \right] \right. \right. \\ & \left. \left. + E_1 \left(\frac{F'_2 C_2}{F_2} - C'_2 \right) - F_1 C_2 \right\} v_{1x} = 0. \end{aligned} \quad (50)$$

The local dispersion relation can be obtained from the coefficients of v_{1x} by the local approximation $dv_{1x}/dx \ll kv_{1x}$,

$$\begin{aligned} & F_2 [F_2 (C_1 F_2 - C_2 F_1) + E_1 (F'_2 C_2 - C'_2 F_2)] \\ & = D_1 [2F'_2 (F'_2 C_2 - C'_2 F_2) - F_2 (F''_2 C_2 - C''_2 F_2)]. \end{aligned} \quad (51)$$

The solutions of local dispersion relation and eigenmode equation agree with each other when the wavenumber k is large and the eigenfunction is spatially localized at a point in x . Equation (51) is an algebraic equation for ω at a point in x and can be solved numerically with the Newton method. In Ref. 10, the local analysis by solving the dispersion relation (51) for equilibrium profiles (44)–(47) shows that the two-fluid MHD and FLR have strong stabilizing effects compared with the three other models and the effect is stronger for higher beta. In this section, we examine the dispersion relation (51) in a wide range of parameters. We assume that the mode is localized at $x = 0$ where the density gradient is maximum. The comparison between local analysis and eigenmode analysis will be shown in Sec. IV.

Figure 2 shows the dependence of the growth rates and the real frequencies on the wavenumber in the MHD model with FLR, $(\lambda, \delta) = (0, 1)$, for $n_2 = 1.1$, and $p_2 = 1.0$. The growth rate shows strong FLR stabilization of large wavenumber modes for $\beta = 0.3$. At the critical wavenumber where the growth rate vanishes, the unstable and stable modes with the same real frequencies and the same amplitudes but opposite signs of growth rates merge and the real frequency bifurcates. However, for smaller β , 0.1 and 0.01, the complete stabilization does not occur. In the case of Fig. 2, we have chosen the case where the pressure gradient is zero, $p'_0 = 0$ as an example that cannot be provided by the equilibrium with a uniform magnetic field as used in Ref. 7

$$P'_0 = \frac{Lg}{V_{Ac}^2} n_0. \quad (52)$$

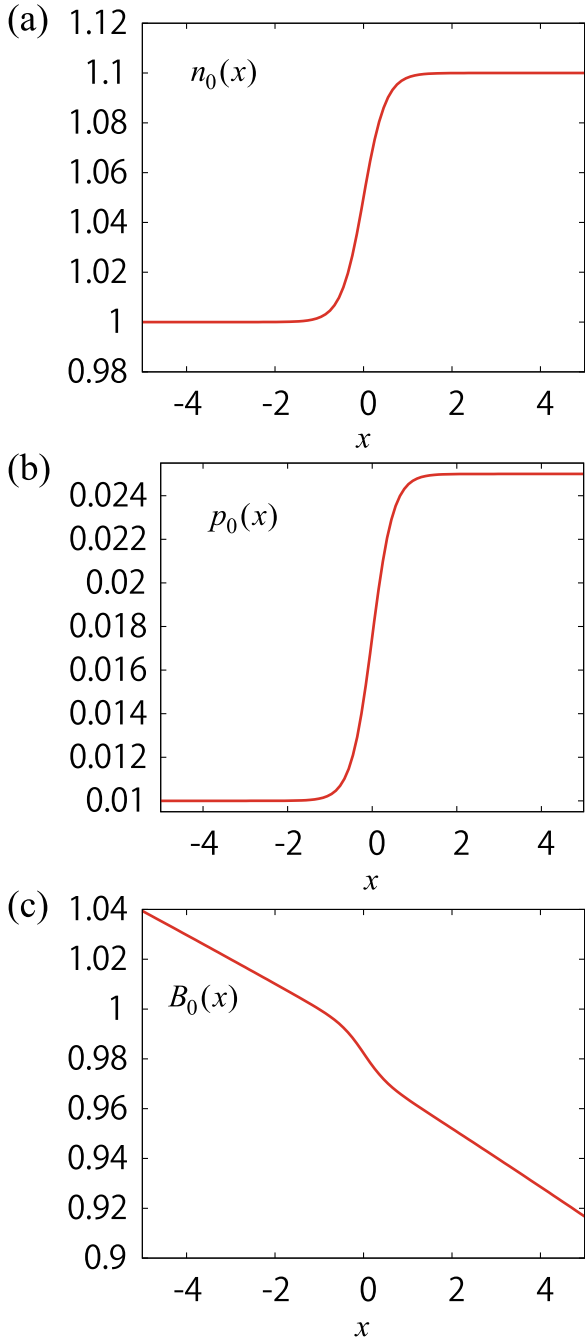


FIG. 1. Equilibrium profiles for the case of $n_2 = 1.1$, $p_2 = 2.5$, and $\beta = 0.01$: (a) the density, (b) the pressure, and (c) the magnetic field.

A simple dispersion relation assuming $v_x \gg v_y$ and omitting higher order derivatives of equilibrium quantities in addition to the local approximation is derived⁷ as

$$\omega(\omega^2 + \omega_{*FLR}\omega + \Gamma_{FLR}^2) + D_{FLR} = 0. \quad (53)$$

The difference between Eqs. (51) and (53) is apparent when both of the two-fluid and FLR effects are included, $(\lambda, \delta) = (1, 1)$. That difference will be discussed later in this section. Here, we use the discussions in Ref. 7 of complete stabilization for general equilibrium (42) based on Eq. (53) for the MHD model with FLR. The condition for complete stabilization by the FLR effect, Eq. (22) of Ref. 7 found from Eq. (53) is written as

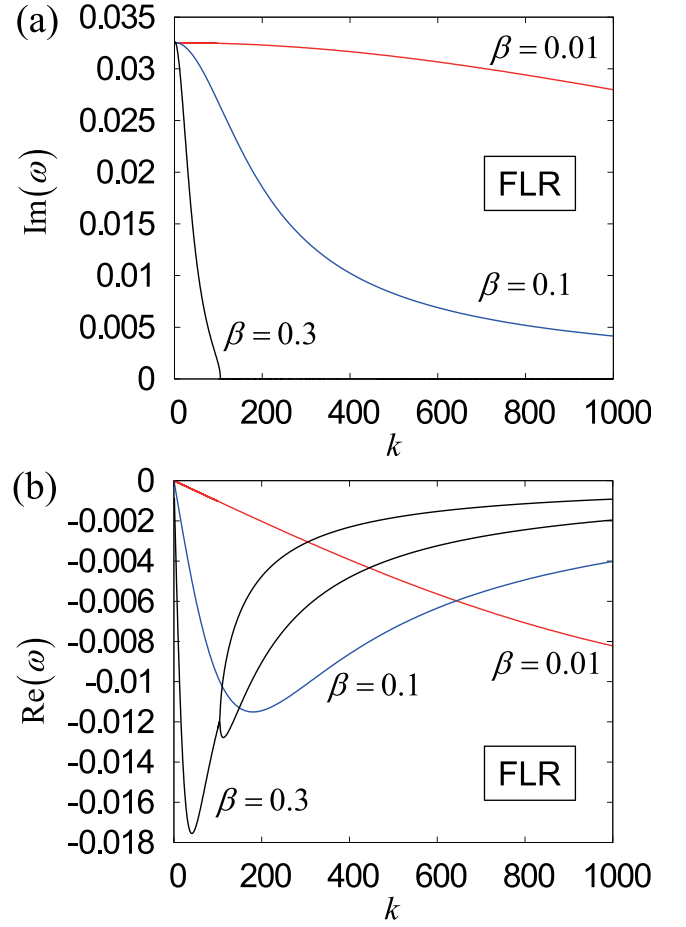


FIG. 2. (a) Growth rates and (b) real frequencies of the RT mode in the MHD model with the FLR term as functions of the wavenumber for different values of β for $n_2 = 1.1$ and $p_2 = 1.0$.

$$\left(\frac{\delta\tau kd_i}{LB_0}\right)^2 \geq \frac{4\left(1 + \frac{\gamma p_0}{B_0^2}\right) \left[\frac{n_0 (Lg/V_{Ac}^2)^2}{B_0^2 1 + \gamma p_0/B_0^2} - \frac{Lg n'_0}{V_{Ac}^2 n_0}\right]}{X}, \quad (54)$$

$$X = \left(1 + \frac{\gamma p_0}{B_0^2}\right) \left[\left(1 + \frac{p_0}{B_0^2}\right) \frac{p'_0}{n_0} - \frac{2 + \gamma p_0/B_0^2 p_0}{1 + \gamma p_0/B_0^2} \frac{Lg}{B_0^2 V_{Ac}^2}\right]^2 - \frac{p_0^2}{B_0^2 n_0} \left[\frac{n_0 (Lg/V_{Ac}^2)^2}{B_0^2 1 + \gamma p_0/B_0^2} - \frac{Lg n'_0}{V_{Ac}^2 n_0}\right]. \quad (55)$$

Since the numerator of the RHS of (54) is positive for the RT mode, the complete stabilization disappears if

$$X \leq 0. \quad (56)$$

Figures 3 and 4 show contours of X of Eq. (55) in (β, p_2) space for $n_2 = 1.1$ and 1.01 , respectively. In the region inside the $X=0$ contour, X is negative and the complete stabilization never occurs. In the region outside, X is positive and the complete stabilization occurs, except for the right side of $B_0 = 0$ line where B_0 becomes imaginary, i.e., β exceeds the equilibrium beta limit. In Fig. 4, the complete stabilization is absent for $\beta \leq 0.277$ at $p_2 = 1.0$. This agrees with Fig. 2. The region of $X < 0$ in Fig. 4 is smaller than that

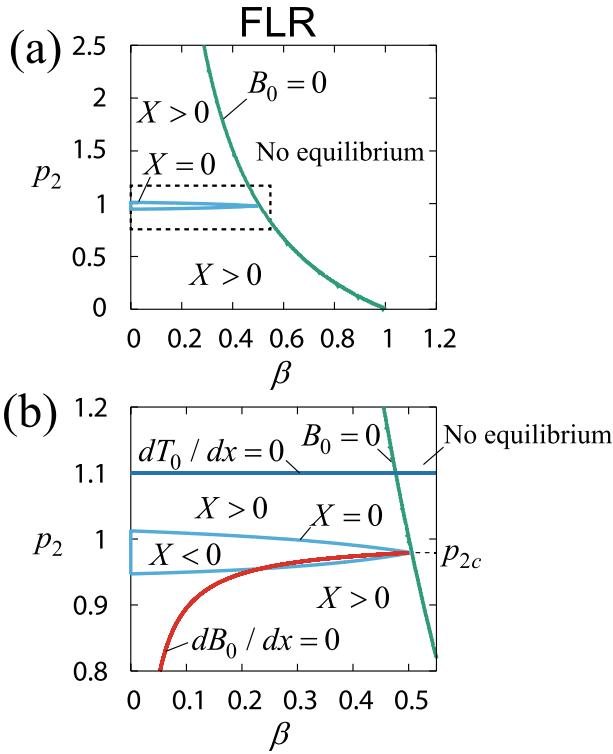


FIG. 3. Contour of X in the $\beta - p_2$ plane for $n_2 = 1.1$. The vicinity of the region where the complete stabilization is absent ($X < 0$) in (a) is enlarged in (b).

in Fig. 3 and complete stabilization occurs for all β within the beta limit at $p_2 = 1.0$. In the low beta limit, $p_0 \ll B_0^2$, Eq. (55) becomes

$$X \simeq \left[\frac{p'_0}{n_0} - \frac{2p_0 Lg}{B_0^2 V_{Ac}^2} \right]^2 \frac{p_0^2}{B_0^2} - \frac{p_0^2}{B_0^2 n_0} \left[\frac{n_0 (Lg)^2}{B_0^2 V_{Ac}^2} - \frac{Lg n'_0}{V_{Ac}^2 n_0} \right]. \quad (57)$$

Substituting (57) into (56), we obtain the condition that complete stabilization does not occur in the low beta limit as

$$\left(\frac{p'_0}{n_0} \right)^2 - \frac{4p_0 Lg p'_0}{B_0^2 V_{Ac}^2 n_0} + \frac{p_0^2 Lg}{B_0^2 n_0 V_{Ac}^2} \left(\frac{3n_0 Lg}{B_0^2 V_{Ac}^2} + \frac{n'_0}{n_0} \right) \leq 0, \quad (58)$$

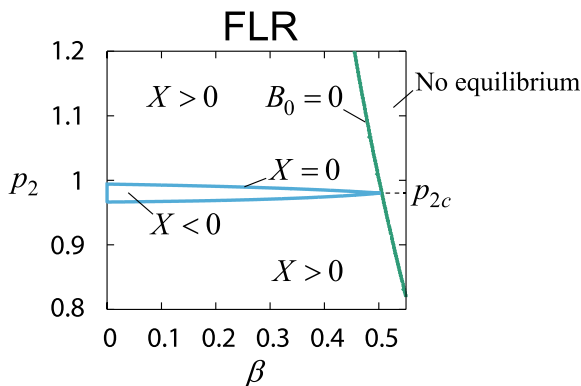


FIG. 4. Contour of X in $\beta - p_2$ plane for $n_2 = 1.01$.

when $p'_0 \approx 0$, (58) yields the condition for the absence of complete FLR stabilization in the limit of low beta and small pressure gradient, assuming $Lg/V_{Ac}^2 < 0$

$$\frac{n'_0}{n_0} + \frac{3n_0 Lg}{B_0^2 V_{Ac}^2} \geq 0, \quad (59)$$

when $\beta = 0$, the LHS is 0.0635 for $n_2 = 1.1$ (Fig. 3) while it is -0.0202 for $n_2 = 1.01$ (Fig. 4). On the other hand, in the high beta limit, $p_0 \gg B_0^2$, Eq. (55) becomes

$$X \simeq \frac{\gamma p_0}{B_0^2} \left(\frac{p_0}{B_0^2} \right)^2 \left(\frac{p'_0}{n_0} - \frac{Lg}{V_{Ac}^2} \right)^2 - \frac{p_0^2}{B_0^2 n_0} \left[\frac{n_0 (Lg)^2}{\gamma p_0 V_{Ac}^2} - \frac{Lg n'_0}{V_{Ac}^2 n_0} \right]. \quad (60)$$

Equation (60) automatically satisfies (56) for equilibrium with uniform magnetic field (52) since the first term vanishes and the second term is negative for the RT instability. When $p'_0 \approx 0$, substituting (60) into (56), assuming $Lg/V_{Ac}^2 < 0$, the condition for the density gradient that causes the absence of the complete FLR stabilization is obtained as

$$\frac{n'_0}{n_0} \geq - \frac{\gamma p_0 n_0 Lg}{B_0^2 B_0^2 V_{Ac}^2}. \quad (61)$$

The density gradient that satisfies (61) becomes very large for the high beta limit. Equation (60) suggests that the absence of complete FLR stabilization for high beta could be prevented by a small gradient of the magnetic field B_0 since the first term of the RHS is proportional to a higher order of p_0 than the second term is. From Eq. (55), X is always negative for RT instability when the equilibrium satisfies

$$\left[\left(1 + \frac{p_0}{B_0^2} \right) \frac{p'_0}{n_0} - \frac{2 + \gamma p_0 / B_0^2 p_0 Lg}{1 + \gamma p_0 / B_0^2 B_0^2 V_{Ac}^2} \right]^2 = 0. \quad (62)$$

In the high beta limit, $p_0 \gg B_0^2$, as in Eq. (60), Eq. (62) coincides with the equilibrium equation with uniform magnetic field (52). Substituting equilibrium profiles (44)–(47) at $x = 0$, Eq. (52) yields

$$p_2 = p_1 + \frac{(x_2 - x_1)(n_1 + n_2) Lg}{2\beta V_{Ac}^2}, \quad (63)$$

when $B_0 \approx 0$, Eq. (47) yields

$$\beta = \frac{B_Z^2}{p_1 + p_2}. \quad (64)$$

Substituting Eq. (64) into Eq. (63), we obtain

$$p_2 = p_{2c} \equiv \frac{\frac{B_Z^2}{x_2 - x_1} + \frac{n_1 + n_2 Lg}{2 V_{Ac}^2}}{\frac{B_Z^2}{x_2 - x_1} - \frac{n_1 + n_2 Lg}{2 V_{Ac}^2}} p_1. \quad (65)$$

Figures 3 and 4 show that at $p_2 = p_{2c}$, $p_{2c} \simeq 0.979$, and 0.980 , respectively, the value of β for $X < 0$ ranges from zero

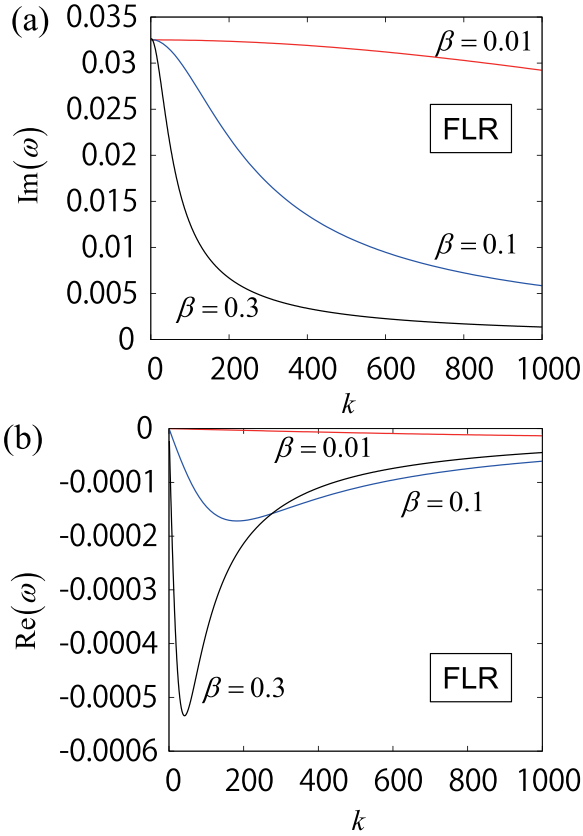


FIG. 5. (a) Growth rates and (b) real frequencies of the RT mode in the MHD model with the FLR term as functions of the wavenumber for different values of β for $n_2 = 1.1$ and $p_2 = 0.97922$.

to the equilibrium beta limit. Figure 5 shows growth rates and real frequencies for $p_2 = p_{2c}$. The complete stabilization and the bifurcation of the real frequency do not occur even for a high beta $\beta = 0.3$. In Fig. 3, the $dB_0/dx = 0$ curve is given by Eq. (63) that locally satisfies Eq. (52) at $x = 0$. For this curve, since the pressure gradient is independent of beta value, p_2 must depend on β . Figure 3 shows that, if we increase β along the $dB_0/dx = 0$ curve, the result of Ref. 7 that the complete FLR stabilization appears for low beta and disappears for high beta can be reproduced. See the Appendix for the relation between β and beta values. At $p_2 = 1.1$ in Fig. 3, the temperature $T_0 \equiv p_0/n_0$ is constant, $dT_0/dx = 0$, and the complete stabilization occurs for all β within the equilibrium beta limit.^{6,7} Figure 6 shows growth rates and real frequencies for this case and the complete stabilization occurs even for a low beta $\beta = 0.01$. Figures 7 and 8 show growth rates and real frequencies for $p_2 = 0.95$ and 0.9, respectively, for $n_2 = 1.1$. For $p_2 = 0.9$, same as for $p_2 = 1.1$, X is always negative and the complete stabilization occurs. For $p_2 = 0.95$, analogous to $p_2 = 1.0$, X is negative for low beta and positive for high beta and the complete stabilization does not appear for the low beta $\beta \leq 0.109$. Real frequencies in Figs. 2 and 5–8 show that the real frequencies increase with p_2 , and are negative for $p_2 < p_{2c}$, close to zero at $p_2 = p_{2c}$ and positive for $p_2 > p_{2c}$.

Here we examine the combination of the FLR and two-fluid effects. We choose $n_2 = 1.1$ and $p_2 = 1.0$ where complete stabilization due to the FLR effect disappears for low

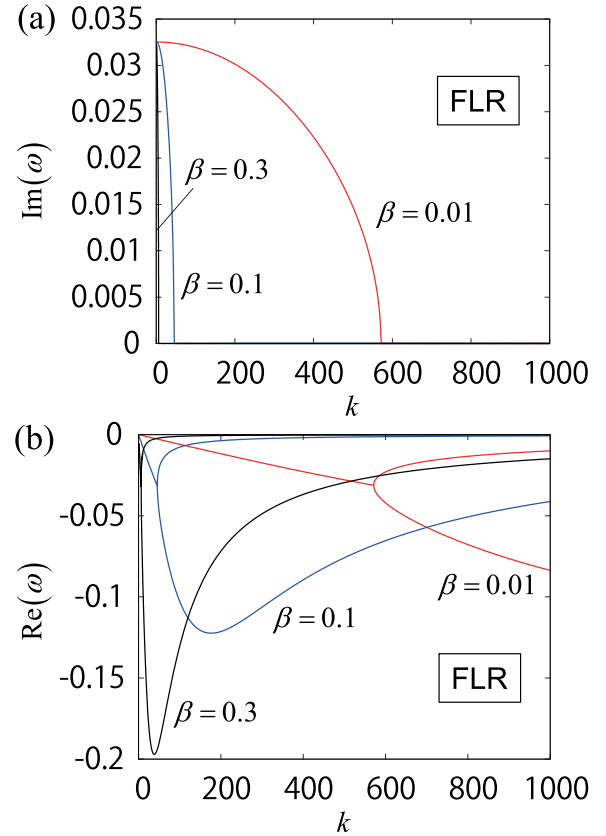


FIG. 6. (a) Growth rates and (b) real frequencies of the RT mode in the MHD model with the FLR term as functions of the wavenumber for different values of β for $n_2 = 1.1$ and $p_2 = 1.1$.

beta, as mentioned above, as an example that shows complicated beta dependence. Figures 9–12 show the growth rates and real frequencies for $\beta = 0.01, 0.1, 0.3$, and 0.36, respectively. We compare the four models, the MHD, $(\lambda, \delta) = (0, 0)$, FLR, $(\lambda, \delta) = (0, 1)$, TF, $(\lambda, \delta) = (1, 0)$, and TF+FLR, $(\lambda, \delta) = (1, 1)$, models with each other. The RT instability in the MHD model is independent of beta and wavenumber, and the frequency is purely imaginary. The four models are not much different for small wavenumber modes but the two-fluid and FLR effects become relevant as the wavenumber increases. For the FLR model, the results of Fig. 2 are used. The two-fluid effect is stabilizing for a low beta $\beta = 0.01$ (Fig. 9), but destabilizing for higher betas $\beta = 0.1, 0.3$, and 0.36 (Figs. 10–12) although the growth rate decreases as β is increased from 0.1. The growth rates for the TF+FLR model for lower betas $\beta = 0.01$ and 0.1 (Figs. 9 and 10) indicate the strong stabilization due to the coupling of FLR and two-fluid effects compared with the sole effect of either two-fluid or FLR. These results are similar to those of Refs. 9 and 10. The complete stabilization occurs in these two cases. In Fig. 10, especially, the two-fluid effect is destabilizing and the mode is completely stabilized by adding the FLR effect. This is similar to the result of Ref. 8. However, the combination of two-fluid and FLR effects is less stabilizing for large wavenumber modes than the FLR effect alone for higher betas $\beta = 0.3$ and 0.36 (Figs. 11 and 12); the complete stabilization disappears for $\beta = 0.3$ (Fig. 11) although it appears again when β is further increased to $\beta = 0.36$ (Fig. 12). The

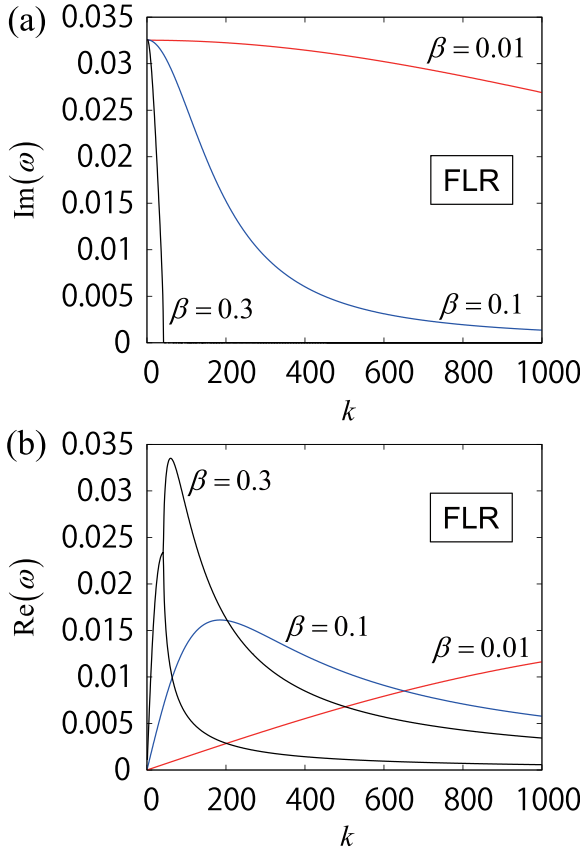


FIG. 7. (a) Growth rates and (b) real frequencies of the RT mode in the MHD model with the FLR term as functions of the wavenumber for different values of β for $n_2 = 1.1$ and $p_2 = 0.95$.

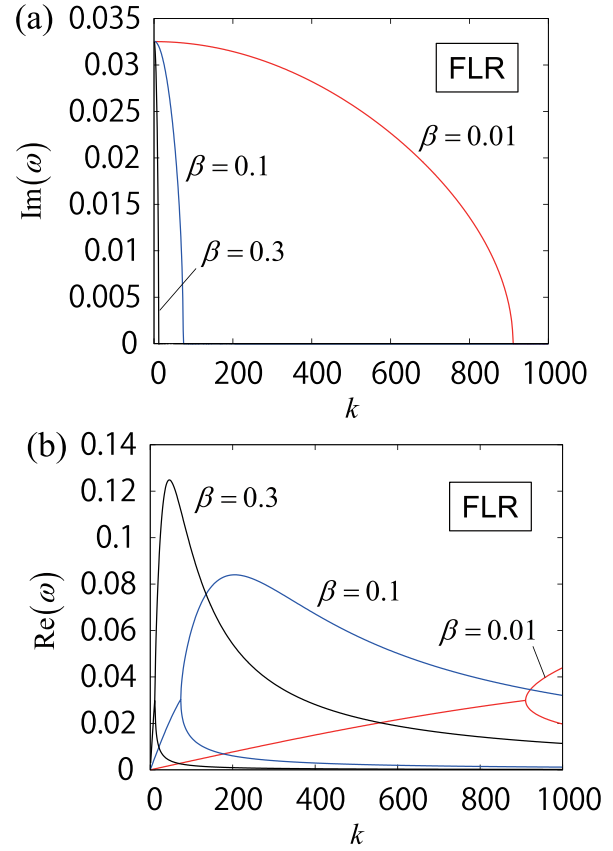


FIG. 8. (a) Growth rates and (b) real frequencies of the RT mode in the MHD model with the FLR term as functions of the wavenumber for different values of β for $n_2 = 1.1$ and $p_2 = 0.9$.

relation between the behaviors of the three models, TF, FLR, and TF+FLR models, is not straightforward although the growth rates and real frequencies of the TF+FLR model are similar to those of the TF model for a low beta $\beta = 0.01$, and similar to those of the FLR model for high betas $\beta = 0.3$ and 0.36 .

It is noted that, for the FLR+TF model, the real frequency indicates complicated bifurcations and multiple unstable modes appear near the marginally stable region for $\beta = 0.1$ (Figs. 10 and 13). In the small wavenumber region, there is another mode close to the RT mode in real frequency and they are coupled with each other near the marginally stable region for the RT mode. In the TF model, $(\lambda, \delta) = (1, 0)$, the RHS of (51) is zero and the LHS is decoupled into two dispersion relations

$$F_2(C_1 F_2 - C_2 F_1) + E_1(F_2' C_2 - C_2' F_2) = 0, \quad (66)$$

$$F_2 = 0. \quad (67)$$

Equation (66) includes RT modes with two-fluid effects. Equation (67) yields the following dispersion relation

$$\begin{aligned} & [n_0 \omega^2 - k^2(\gamma p_0 + B_0^2)] \left(\omega - \lambda k \frac{d_i n_0'}{L n_0^2} B_0 \right) \\ & - \lambda k^3 \frac{d_i B_0}{L n_0} \left[B_0^2 \left(\frac{n_0'}{n_0} - \frac{B_0'}{B_0} \right) + (1 - \tau) \left(\frac{n_0'}{n_0} \gamma p_0 - p_0' \right) \right] = 0, \end{aligned} \quad (68)$$

which includes the high frequency mode like the fast magnetosonic wave

$$\omega^2 \simeq k^2(\gamma p_0 + B_0^2)/n_0,$$

and the low frequency mode like the electron drift wave

$$\begin{aligned} \omega \simeq \omega_{*e} \equiv & \lambda k \frac{d_i B_0}{L n_0} \\ & \times \frac{\gamma p_0 (n_0'/n_0) + B_0 B_0' + (1 - \tau)[p_0' - \gamma p_0 (n_0'/n_0)]}{\gamma p_0 + B_0^2}. \end{aligned} \quad (69)$$

Figure 13 shows that, in the small wavenumber region, the dispersion relation (69) agrees well with that of the mode that is coupled with the RT mode. Figure 13 also shows that the dispersion relation (51) contains the ion drift wave as well, but it is not coupled in this case. The dispersion relation (53) does not include the electron drift wave and such coupling is not found (see Fig. 14), while the dispersion relation (53) includes the ion drift wave, which is also coupled with the RT mode in some cases.¹²

IV. EIGENMODE ANALYSIS

Here, we examine the eigenmodes of the RT instability to compare with the spatial dependence of local analysis.

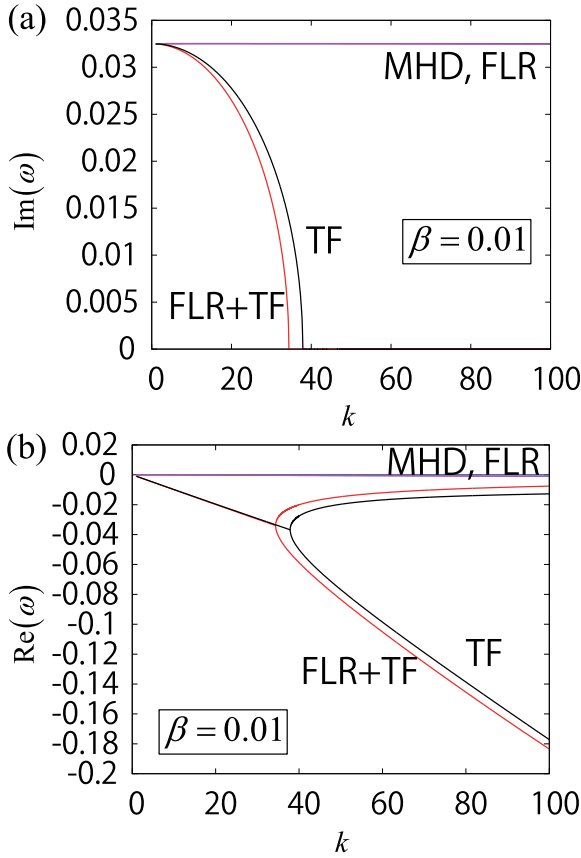


FIG. 9. (a) Growth rates and (b) real frequencies of the RT mode as functions of the wavenumber for different MHD models for $n_2 = 1.1$, $p_2 = 1.0$, and $\beta = 0.01$.

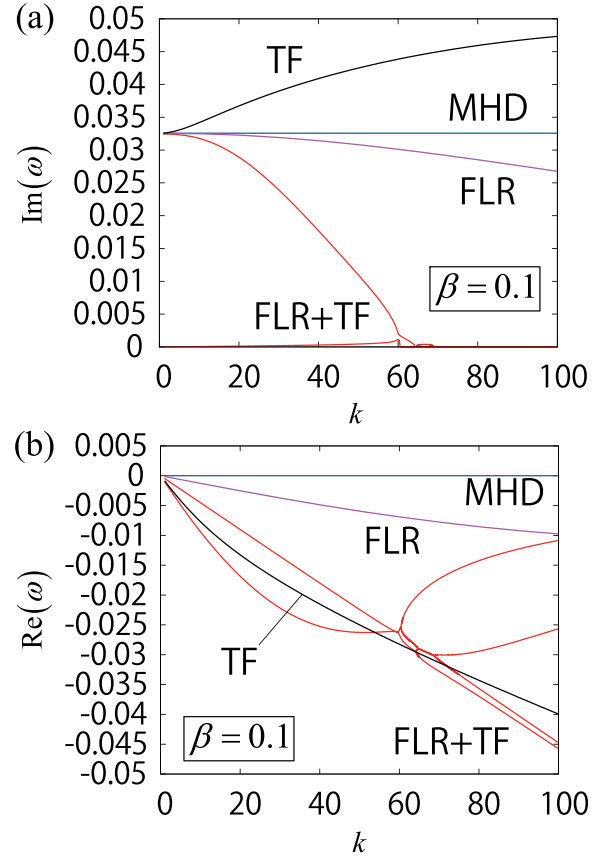


FIG. 10. (a) Growth rates and (b) real frequencies of the RT mode as functions of the wavenumber for different MHD models for $n_2 = 1.1$, $p_2 = 1.0$, and $\beta = 0.1$.

When the FLR effect is included, $\delta = 1$, we solve the two coupled second-order ODEs (29) and (30) with the fixed boundary condition for v_{1x} ,

$$v_{1x} = 0, \tag{70}$$

and another boundary condition

$$B_2(x)v'_{x1} + C_2(x)v_{x1} + F_2(x)v_{y1} = 0. \tag{71}$$

The second condition (71) is obtained from Eq. (30) assuming that v''_{1x} that arises due to the FLR effect is small in regions far from the center, $x=0$. Equations (29) and (30) are numerically solved for the FLR model, $(\lambda, \delta) = (0, 1)$, and the TF+FLR model, $(\lambda, \delta) = (1, 1)$, by taking finite differences and finding eigenvalues of ω from the determinant of the matrix equation for discretized variables v_{x1} and v_{y1} . When the FLR effect is omitted, $\delta = 0$, Eq. (50) reduces to the second-order ODE, since $D_1 = A_2 = 0$

$$\begin{aligned} &(A_1F_2 - E_1B_2)v''_{1x} \\ &+ \left[B_1F_2 + E_1 \left(\frac{F'_2B_2}{F_2} - B'_2 - C_2 \right) - F_1B_2 \right] v'_{1x} \\ &+ \left[C_1F_2 + E_1 \left(\frac{F'_2C_2}{F_2} - C'_2 \right) - F_1C_2 \right] v_{1x} = 0. \end{aligned} \tag{72}$$

We solve Eq. (72) numerically with the shooting method for the MHD model, $(\lambda, \delta) = (0, 0)$, and the TF model, $(\lambda, \delta) = (1, 0)$, with the fixed boundary condition for v_{1x} , (70). In this study, we set the numerical domain as $-\pi/4 \leq x \leq \pi/4$ with 1000 intervals. Figures 15–18 show the growth rates and real frequencies of eigenmodes for the four models as functions of the wavenumber in comparison with those of local modes at $x=0$ for $n_1 = 1.1$, $p_2 = 2.5$, and $\beta = 0.01$. For large wave number modes found from the local dispersion relation (51), the complete stabilization occurs for the FLR model (Fig. 17), in agreement with Fig. 3, and for the TF+FLR model (Fig. 18) as well while the growth rate is independent of the wavenumber for the MHD model (Fig. 15) and it is reduced but asymptotically approaches a constant for the TF model (Fig. 16). These results for local modes are also shown in Ref. 10 to compare with the simulation results. In the small wavenumber region, the growth rates of the eigenmodes of the RT mode for all of the four models increase with an increase of the wavenumber from the smaller values than those of the local modes. As the wavenumber further increases, the growth rates of the eigenmodes asymptotically become close to those of the local modes except for the FLR model (Fig. 17), where the growth rate of the eigenmode exceeds that of the local mode for $k \geq 36$. The real frequencies of the eigenmodes are not much different from those of local modes for the whole

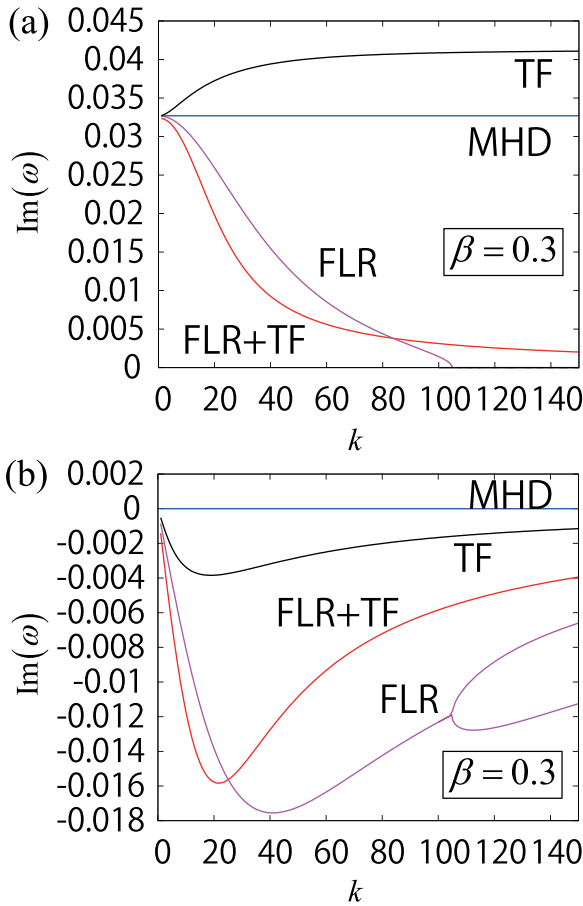


FIG. 11. (a) Growth rates and (b) real frequencies of the RT mode as functions of the wavenumber for different MHD models for $n_2 = 1.1$, $p_2 = 1.0$, and $\beta = 0.3$.

wavenumber regions except for the large wavenumber region of the FLR model. Figures 19–22 show eigenfunctions of v_{1x} for different wavenumbers $k = 1, 10, 20$, and 50 for the MHD, FLR, and TF models and $k = 1, 10$, and 20 for the TF+FLR model where the RT mode is stabilized at $k = 50$. For $k = 1$, the eigenfunctions of all of the four models are broad and the real parts are dominant. For the MHD, TF, and TF+FLR models (Figs. 19, 20, and 22, respectively), the eigenfunctions become localized near the center as the wavenumber increases although the imaginary parts of v_{1x} become dominant for the TF and TF+FLR models while v_{1x} has only the real part for the MHD model. Thus, the local modes are well approximated with the eigenmodes in the large wavenumber region for these three models. On the other hand, for the FLR model (Fig. 21), the eigenfunctions are broad and the growth rates and the real frequencies for the eigenmodes and the local modes are different even for large wavenumbers.

In order to explain the difference between the local dispersion relation and eigenmodes as deviation from the assumption of local analysis that the eigenfunction is localized at the center in more detail, we examine the spatial dependence of frequencies found from the local dispersion relation in comparison with the shape of eigenfunctions. Figures 23–26 show the growth rates and real frequencies

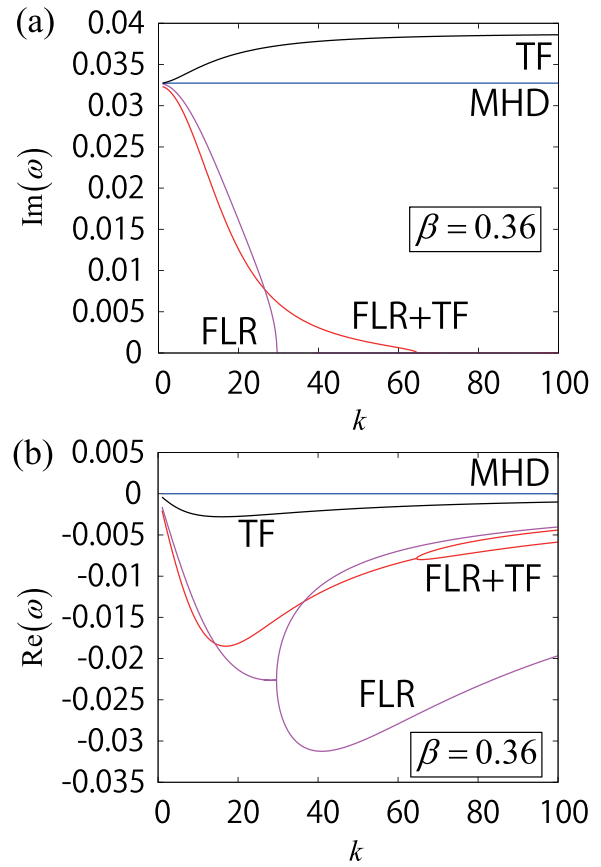


FIG. 12. (a) Growth rates and (b) real frequencies of the RT mode as functions of the wavenumber for different MHD models for $n_2 = 1.1$, $p_2 = 1.0$, and $\beta = 0.36$.

found from the local dispersion relation (51) at each point of x for different values of the wavenumber for each model. The local frequency for the MHD model has only the imaginary part, does not depend on the wavenumber everywhere in x , and is peaked at the center, $x = 0$ (Fig. 23). The eigenfunctions are broader for smaller wavenumbers (Fig. 19), extending to the regions of x where the local growth rates shown in Fig. 23 are lower, and, thus, the growth rate of the eigenmode is smaller than that of the local dispersion relation at the center. On the other hand, the eigenfunctions

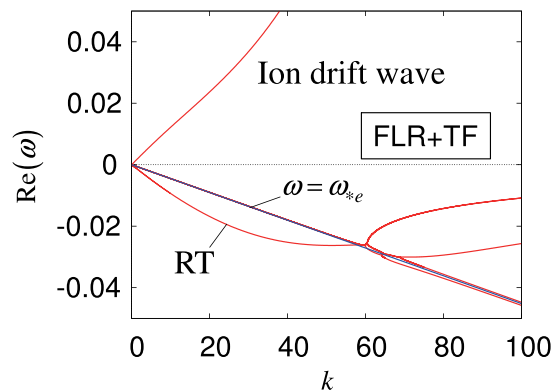


FIG. 13. Real frequencies for the FLR+TF model and $\omega = \omega_{*e}$ as functions of the wavenumber for $n_2 = 1.1$, $p_2 = 1.0$, and $\beta = 0.1$.

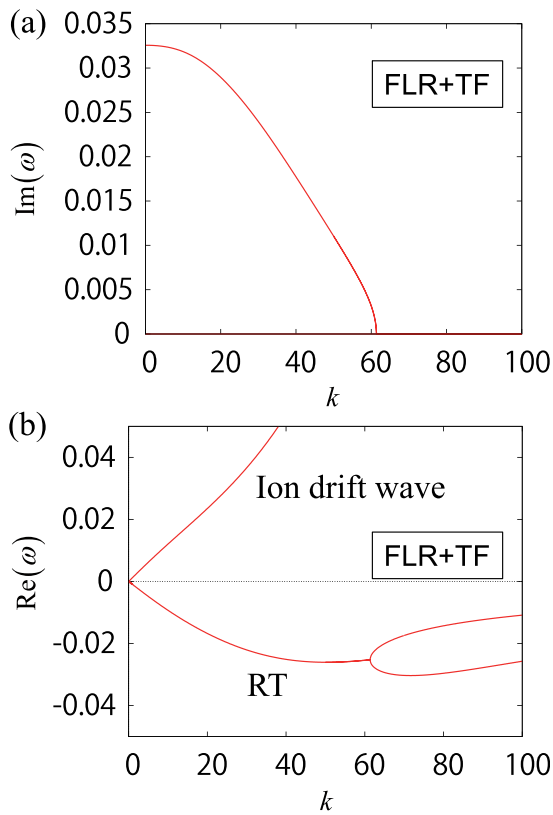


FIG. 14. (a) Growth rate and (b) real frequencies of the RT mode and ion drift wave as functions of the wavenumber for the FLR+TF model given by Eq. (53) for $n_2 = 1.1$, $p_2 = 1.0$, and $\beta = 0.1$.

are narrower for larger wavenumbers, localized near the center where the growth rate is maximum, and the growth rate of the eigenmode asymptotically becomes close to those of the local modes at the center. For the TF model, the local frequencies have both of the real and imaginary parts, and the growth rates are peaked at the center and decreases with the increase of the wavenumber everywhere in x while real frequencies for unstable mode do not depend on x compared with the growth rates (Fig. 24). The eigenfunctions have

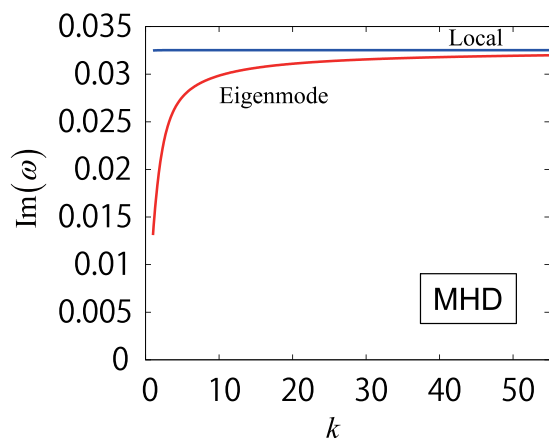


FIG. 15. Growth rates of the RT mode as functions of the wavenumber for the MHD models in comparison between eigenmode and local analyses for $n_1 = 1.1$, $p_2 = 2.5$, and $\beta = 0.01$.

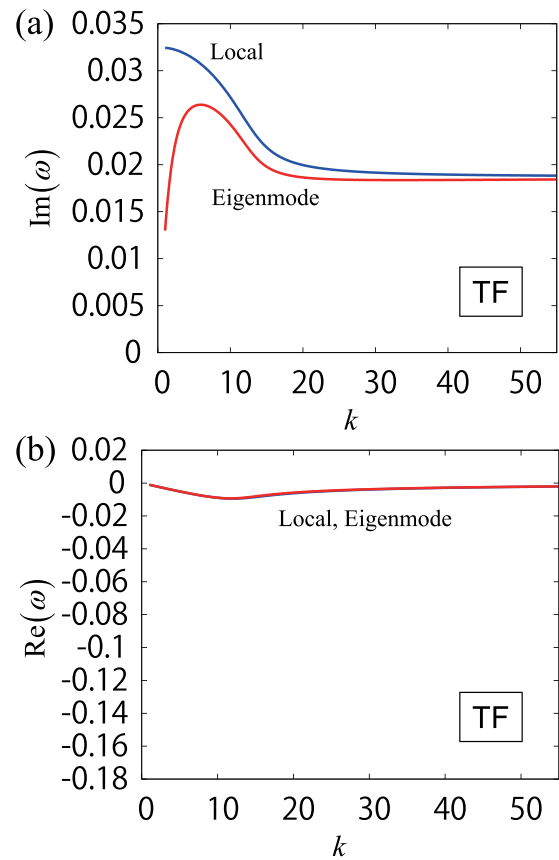


FIG. 16. (a) Growth rates and (b) real frequencies of the RT mode as functions of the wavenumber for the two-fluid MHD model in comparison between eigenmode and local analyses for $n_1 = 1.1$, $p_2 = 2.5$, and $\beta = 0.01$.

both of the real and imaginary parts but the dependence of the absolute values of the eigenfunctions on the wavenumber is similar to those of the MHD model (Fig. 20). Thus the growth rate of the eigenmode for the TF model also becomes close to those of the local modes at the center and the real frequencies of the local and eigenmode analyses are not much different in the whole wavenumber region. For the FLR model, the local growth rate is peaked at the center for small wavenumbers $k = 1$ and 10 (Fig. 25). The growth rate near the center decreases as the wavenumber increases and for $k = 50$, where the wavenumber is slightly larger than the critical wavenumber for the complete stabilization at the center, the edge regions are still unstable (Fig. 25). The eigenfunction for the FLR model is broad as for the MHD model for $k = 1$ (Fig. 21). As the wavenumber increases, the eigenfunction becomes more localized (see $k = 10$ in Fig. 21). However, when the wavenumber further increases, the eigenfunction becomes broad again and finally has two humps at both sides (see $k = 50$ in Fig. 21), where the local growth rate is still positive. This may cause the larger growth rate of the eigenmode than that of the local growth rate at the center in the large wave number region. The spatial dependence of the local real frequencies becomes relevant as the wavenumber increases and the difference between the real frequencies of the local mode at the center and the eigenmode arises due to the broad eigenfunctions in the large

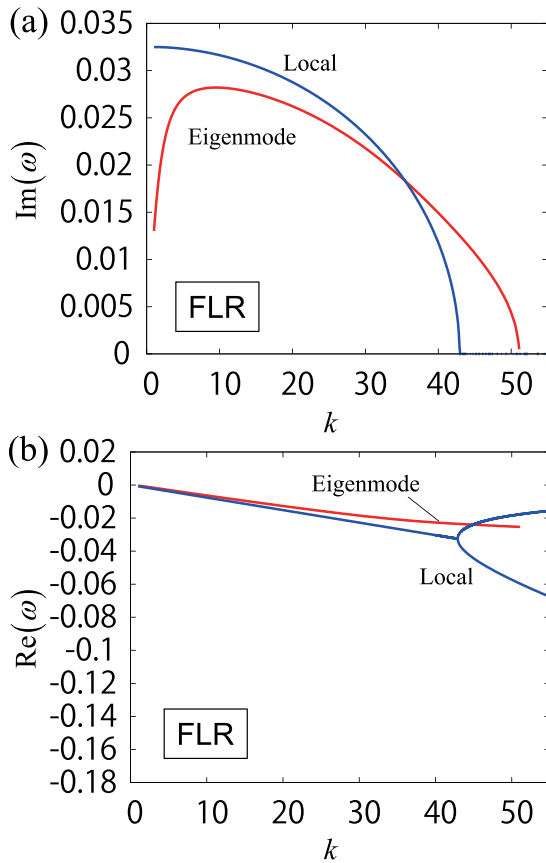


FIG. 17. (a) Growth rates and (b) real frequencies of the RT mode as functions of the wavenumber for the MHD models with the FLR effect in comparison between eigenmode and local analyses for $n_1 = 1.1$, $p_2 = 2.5$, and $\beta = 0.01$.

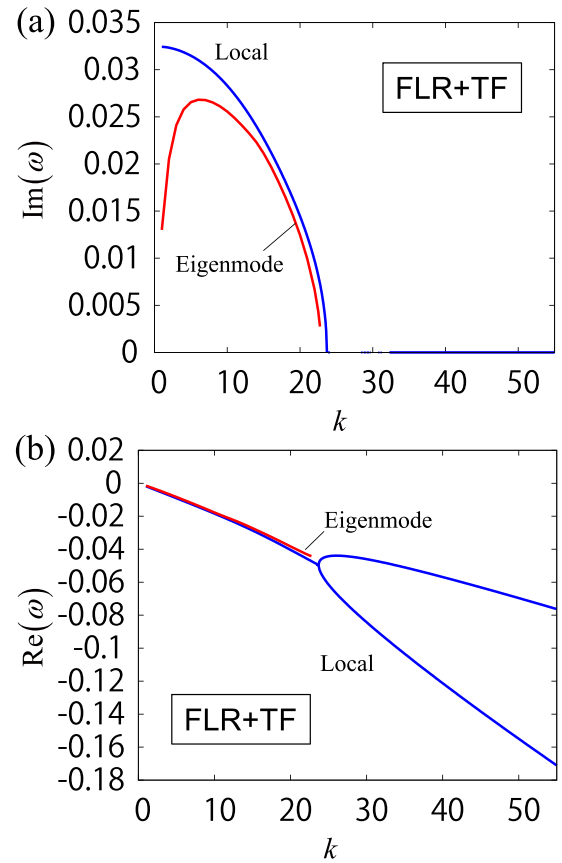


FIG. 18. (a) Growth rates and (b) real frequencies of the RT mode as functions of the wavenumber for the two-fluid MHD model with the FLR effect in comparison between eigenmode and local analyses for $n_1 = 1.1$, $p_2 = 2.5$, and $\beta = 0.01$.

wave number region. For the FLR+TF model, the local growth rates are peaked at the center and decrease with the increase of the wavenumber everywhere in x and the local real frequencies for unstable mode do not depend on x compared to the growth rates (Fig. 26) as for TF model. The dependence of the absolute values of the eigenfunctions on the wavenumber for the TF+FLR model is similar to those of the MHD and TF models (Fig. 22). Thus the growth rate of the eigenmode for the TF+FLR model also becomes close to those of the local modes at the center and the real frequencies of the local and eigenmode analyses are not much different in the whole wavenumber region. The eigenmode analysis presented here qualitatively agrees with nonlinear simulation results in Ref. 10 although the numerical domain is narrower for eigenmode analysis, which may affect modes with broad eigenfunctions, and nonlinear simulation contains numerical dissipation for large wave numbers.

V. SUMMARY AND DISCUSSION

We have shown the parameter dependence of two-fluid and FLR effects on the RT instability in finite beta plasmas by using extended MHD models. The beta dependence has been studied in detail by local analysis. In equilibria with nonuniform temperature and magnetic fields, the absence of complete stabilization of large wavenumber modes due to

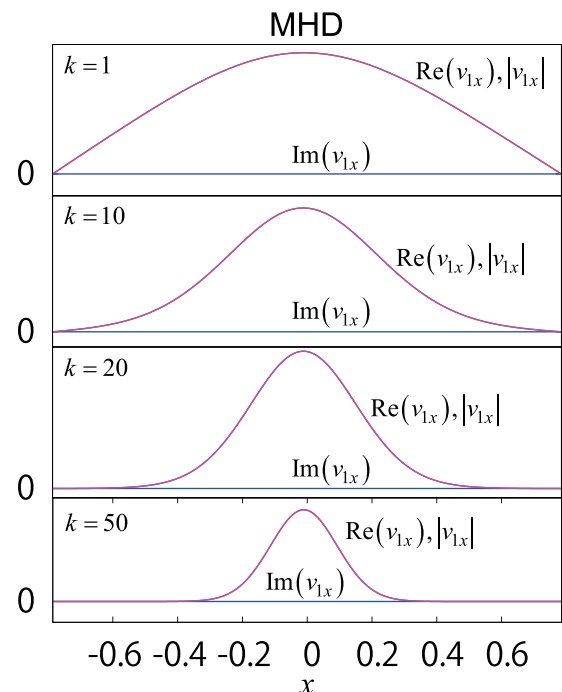


FIG. 19. Eigenfunctions of the RT mode for different wavenumbers for the MHD model in Fig. 15.

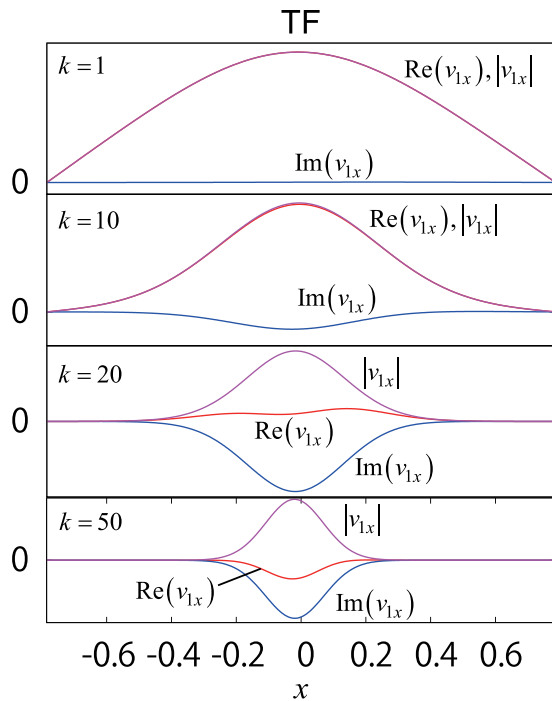


FIG. 20. Eigenfunctions of the RT mode for different wavenumbers for the TF model in Fig. 16.

the FLR effect occurs for beta lower than the critical value for small pressure gradient. When the pressure gradient is equivalent to that of the equilibria with uniform magnetic field, the critical beta value coincides with the equilibrium beta limit. The sign of real frequency becomes opposite

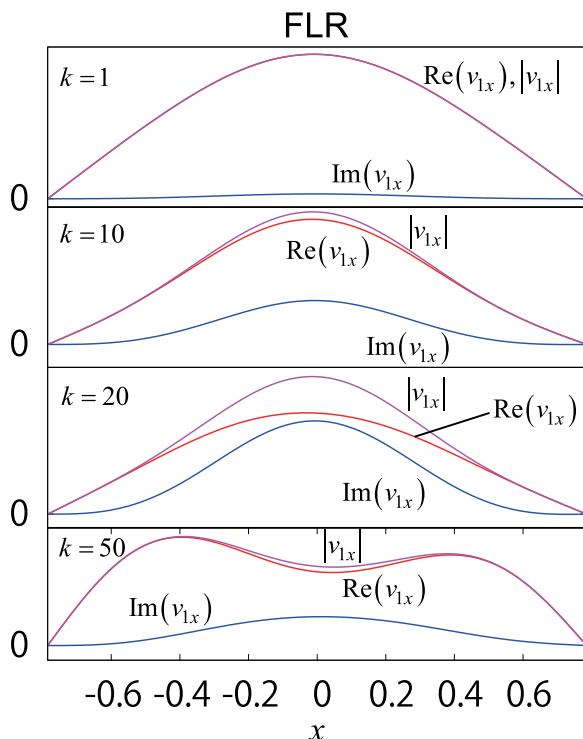


FIG. 21. Eigenfunctions of the RT mode for different wavenumbers for the FLR model in Fig. 17.

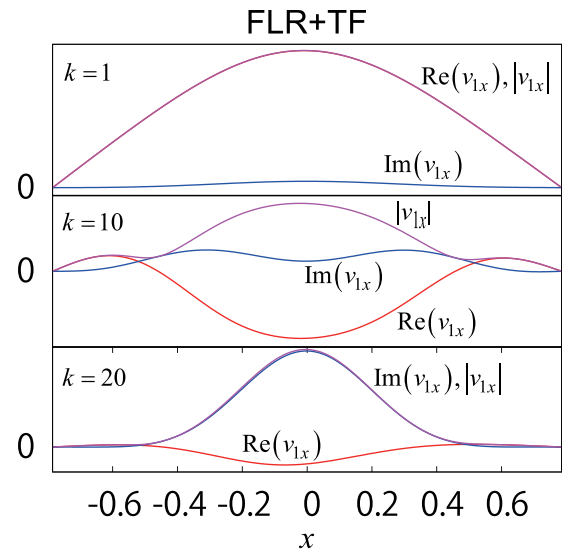


FIG. 22. Eigenfunctions of the RT mode for different wavenumbers for the FLR+TF model in Fig. 18.

when the pressure gradient is varied across this value. These results stem from equilibria with nonuniform magnetic field where pressure gradient and density gradient can be independently given. The combination of two-fluid and FLR effects can also cause the absence of complete stabilization and the two-fluid MHD model with FLR is not always most stable among the MHD model, two-fluid MHD model, and MHD model with FLR but it depends on beta. The two-fluid MHD model with FLR also shows coupling between the RT mode and the electron drift-like wave. Spatial dependence of the local modes is examined in comparison with that of eigenmodes. For the MHD model with FLR, for large wavenumber modes, the eigenmode is more unstable than the local mode since the eigenfunction has two humps in the region that is still unstable while the RT mode is completely stabilized at the center in the local analysis.

These results may be useful for nonlinear extended MHD simulations. It is noted, however, that simplifications

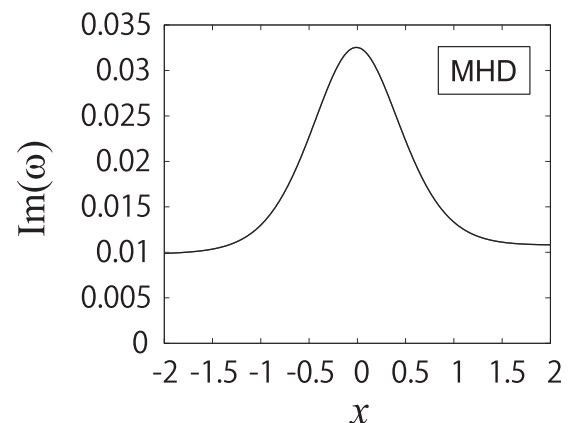


FIG. 23. Spatial dependence of the local growth rates of the RT mode for the MHD model for parameters of Fig. 15.

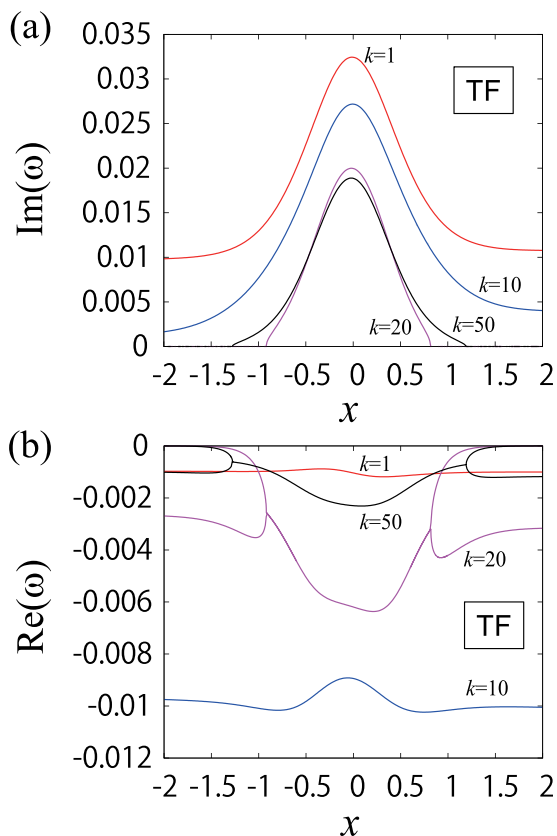


FIG. 24. Spatial dependence of (a) the local growth rates and (b) the local real frequencies for the TF model for parameters of Fig. 16.

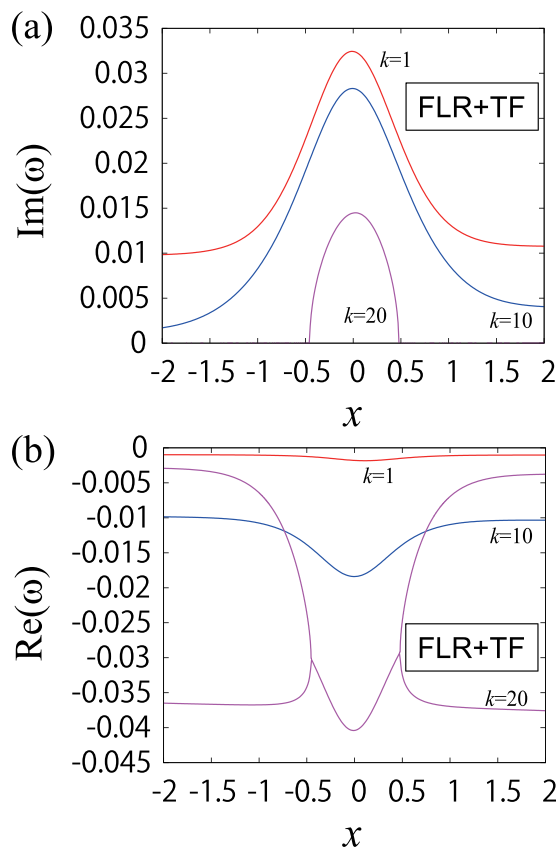


FIG. 26. Spatial dependence of (a) the local growth rates and (b) the local real frequencies for the FLR+TF model for parameters of Fig. 18.

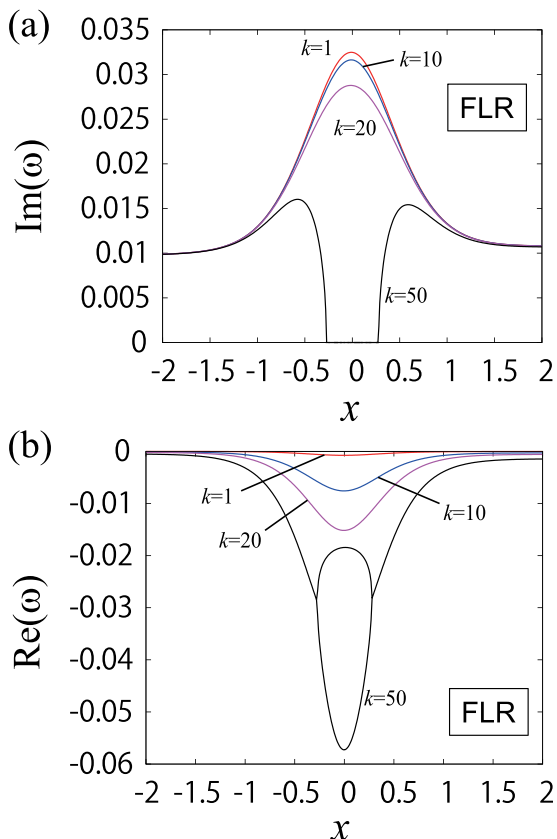


FIG. 25. Spatial dependence of (a) the local growth rates and (b) the local real frequencies for the FLR model for parameters of Fig. 17.

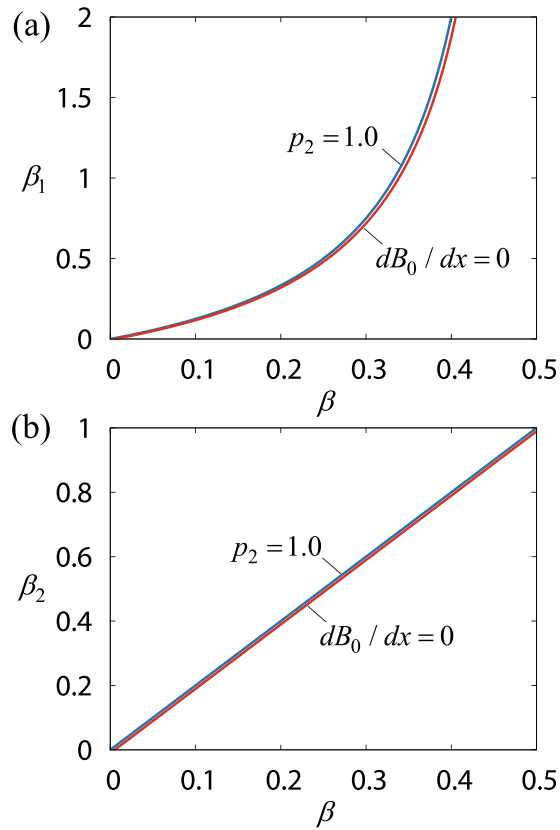
we have adapted according to the previous studies^{1,7} should be examined in future studies. The simple equation for electron pressure where total pressure of ions and electrons is adiabatic and the ratio between ion and electron pressures is constant may not give a proper Doppler shift due to the difference between ion and electron flows. In the present results, this may especially affect the dispersion for the electron drift wave. The parallel and perpendicular heat fluxes are omitted in the present model and should be studied using more rigorous fluid moment equations such as in Ref. 14. The effect of the gyroviscosity may be modified in more complicated geometry. The behavior in large wavenumber regions should be examined with kinetic theory.

ACKNOWLEDGMENTS

This work was partially supported by the NIFS Collaborative Research Program (NIFS12KNTS021) and Grant-in-Aid for Scientific Research, KAKENHI (Nos. 23540583 and 24740375).

APPENDIX: RELATION BETWEEN β AND BETA VALUES

Relation between β in Eq. (46) and two types of the beta value for the equilibrium profiles (44)–(47) at $x=0$ are given by

FIG. 27. (a) β_1 and (b) β_2 as functions of β for $n_2 = 1.1$.

$$\beta_1 \equiv \frac{p_0(0)}{B_0^2(0)} = \frac{\beta}{2B_z^2 - \beta(p_1 + p_2)},$$

$$\beta_2 \equiv \frac{p_0(0)}{B_0^2(0)/2 + p_0(0)} = \frac{\beta(p_1 + p_2)}{B_z^2}.$$

Figure 27 shows β_1 and β_2 as functions of β . Two curves for $p_2 = 1.0$ and p_2 for $dB_0/dx = 0$ at x , Eq. (63), are plotted.

¹K. V. Roberts and J. B. Taylor, *Phys. Rev. Lett.* **8**, 197 (1962).

²S. I. Braginskii, in *Reviews of Plasma Physics*, edited by M. A. Leontovich (Consultants Bureau, New York, 1965), Vol. 1, p. 205.

³D. D. Schnack, D. C. Barnes, D. P. Brennan, C. C. Hegna, E. Held, C. C. Kim, S. E. Kruger, A. Y. Pankin, and C. R. Sovinec, *Phys. Plasmas* **13**, 058103 (2006).

⁴J. D. Huba, *Phys. Plasmas* **3**, 2523 (1996).

⁵J. D. Huba and D. Winske, *Phys. Plasmas* **5**, 2305 (1998).

⁶N. M. Ferraro and S. C. Jardin, *Phys. Plasmas* **13**, 092101 (2006).

⁷P. Zhu, D. D. Schnack, F. Ebrahimi, E. G. Zweibel, M. Suzuki, C. C. Hegna, and C. R. Sovinec, *Phys. Rev. Lett.* **101**, 085005 (2008).

⁸P. W. Xi, X. Q. Xu, T. Y. Xia, W. M. Nevins, and S. S. Kim, *Nucl. Fusion* **53**, 113020 (2013).

⁹R. Goto, H. Miura, A. Ito, M. Sato, and T. Hatori, *Plasma Fusion Res.* **9**, 1403076 (2014).

¹⁰R. Goto, H. Miura, A. Ito, M. Sato, and T. Hatori, *Phys. Plasmas* **22**, 032115 (2015).

¹¹A. Ito, R. Goto, T. Hatori, H. Miura, and M. Sato, in *International Sherwood Fusion Theory Conference, New York* (2015).

¹²E. C. Howell and C. R. Sovinec, in *International Sherwood Fusion Theory Conference, New York* (2015).

¹³J. J. Ramos, *Phys. Plasmas* **12**, 112301 (2005).

¹⁴J. J. Ramos, *Phys. Plasmas* **12**, 052102 (2005).